ASSESSING GNSS CARRIER-TO-NOISE-DENSITY RATIO ESTIMATION IN THE PRESENCE OF MEACONER INTERFERENCE

Emile GHIZZO, Axel GARCIA PENA, Julien LESOUPLE, Carl MILNER, Christophe MACABIAU

ENAC, Université de Toulouse, 7 Avenue Edouard Belin, 31400 Toulouse, France

ABSTRACT

In the context of Global Navigation Satellite Systems (GNSS), the measure of the Carrier-to-Noise Density Ratio (C/N_0) plays a critical role in evaluating received signal quality, particularly in the presence of Radio-Frequency Interferences such as from a meaconer. This paper presents a dual-step strategy to characterize C/N_0 under meaconer influence. First, the theoretical expression of the real C/N_0 is computed. Second, a model to predict meaconer-induced distortion on the Moment Method (MM) and the Narrowband-Wideband Power Ratio (NWPR) estimators is derived. The comparison between real and estimated C/N_0 reveals a deviation between NWPR, MM and real C/N_0. In essence, this work enhances comprehension of meaconing-induced C/N_0 distortion.

Index Terms— Global Navigation Satellite Systems (GNSS), Carrier-to-Noise Density Ratio (C/N_0), Jamming, Spoofing, Multipath

1. INTRODUCTION

The C/N_0 parameter is used to detect signal quality degradation for each tracked satellite, aiding in monitoring GNSS receiver aspects like satellite selection and lock status [1, 2]. C/N_0 estimation, obtained from algorithms such as Narrowband-Wideband Power Ratio (NWPR), Beaulieu's, or Moment Method (MM) [3], is then crucial for GNSS signal processing and position estimation. Factors affecting C/N_0 reduction include non-line-of-sight (NLOS), synchronization mismatches, low-elevation antenna gain and Radio-Frequency Interferences (RFI). An example of RF interferer is the meaconer, also known as a GNSS repeater. It is an electronic device designed to capture (with a first receiving antenna), amplify, and rebroadcast electromagnetic signals (with a second emitting antenna) around a given GNSS central frequency [4].

The C/N_0 metric has frequently been used in the literature for detecting spoofing and meaconing interferences [5–9]. However, to the best of the authors' knowledge, a comprehensive analysis of how meaconers impact the estimated C/N_0 has not yet been put forth. This paper employs a dual-step strategy: presenting a theoretical model for the real C/N_0 under meaconer influence, and deriving a model of the meaconer-induced distortion on C/N_0 estimation algorithms, which eases comparison between estimated and real values.

The structure of the paper is as follows. Sec. 2 outlines the correlator output expression. To facilitate the analysis of meaconer influence, it categorizes its impact on the correlator output into four situations: nominal, jamming, spoofing, and multipath. The theoretical expression of real C/N_0 is introduced in Sec. 3. Sec. 4 derives a model to predict meaconer-induced distortion on C/N_0 estimation methods. Lastly, simulation evaluations in Sec. 5 validate and compare the real and estimated C/N_0.

2. CORRELATOR OUTPUT MODEL

Introducing the nominal received GNSS signal r_a at the RF Front-End (RFFE) output, defined by its equivalent baseband model as [10, p. 248]

$$r_a\left(t, \boldsymbol{\eta}_a\right) = \sqrt{C_a}d(t-\tau_a)\left(c * h_{\mathrm{RF}}\right)(t-\tau_a)e^{j\theta_a} \quad (1)$$

where $d(t)$ is the random BPSK navigation signal, $c(t)$ the Pseudo-Random Noise (PRN) signal, h_{RF} the RFFE's impulse response and $\boldsymbol{\eta}_a = [\tau_a, \theta_a, f_a, C_a]$ the time varying nominal parameters, containing respectively the group delay, phase delay, Doppler shift, and received power. The meaconing signal r_s is a repeated version of the nominal signal,

$$\begin{aligned} r_s\left(t, \boldsymbol{\eta}_a, \Delta\boldsymbol{\eta}\right) = {} & \sqrt{\Delta g\, C_a}\, d(t-\tau_a - \Delta\tau) \\ & \times \left(c * h_{\mathrm{RF}}\right)(t-\tau_a - \Delta\tau)e^{j(\theta_a + \Delta\theta)} \end{aligned} \quad (2)$$

where $\Delta\boldsymbol{\eta} = [\Delta\tau, \Delta\theta, \Delta f, \Delta g]$ is the time-varying relative parameters between nominal and meaconer signal, including relative delay, relative phase, relative frequency, and relative power. Finally, let us consider the complex Additive White Gaussian Noise (AWGN) denoted as n, comprising natural AWGN along with additional AWGN re-radiated by the meaconer. The power spectral density (PSD) of n is defined as

$$G_n(f) = |H_{\mathrm{RF}}(f)|^2 N_0\left(1 + \Delta N\right) \quad (3)$$

with $H_{\mathrm{RF}}(f)$ the RFFE's transfer function, N_0 the nominal noise PSD, and ΔN the relative PSD between natural and re-radiated AWGN. The complete received signal r at the RFFE output can then be expressed as

$$r(t, \boldsymbol{\eta}_a, \Delta\boldsymbol{\eta}) = r_a\left(t, \boldsymbol{\eta}_a\right) + r_s\left(t, \boldsymbol{\eta}_a, \Delta\boldsymbol{\eta}\right) + n(t). \quad (4)$$

In GNSS receivers, C/N_0 estimation often relies on the post-correlation signal. This involves correlating r with a local replica over the integration time T_i, as defined for epoch k by

$$\lambda[k, \varepsilon_{\boldsymbol{\eta}}, \Delta\boldsymbol{\eta}] = \frac{1}{T_i} \int_{\hat{\tau}+kT_i}^{\hat{\tau}+(k+1)T_i} r(t, \boldsymbol{\eta}_a, \Delta\boldsymbol{\eta})c^\star(t-\hat{\tau})e^{-j\hat{\theta}}dt \quad (5)$$

where * denotes the complex conjugate. Throughout the paper, $\boldsymbol{\eta}_a[k]$ and $\Delta\boldsymbol{\eta}[k]$ refer to continuous-time parameters $\boldsymbol{\eta}_a(t)$ and $\Delta\boldsymbol{\eta}(t)$ at $t = (k + 1/2)T_i$, $\hat{\boldsymbol{\eta}}[k] = [\hat{\tau}, \hat{\theta}, \hat{f}]$ denotes tracking estimates and $\varepsilon_{\boldsymbol{\eta}}[k] = \boldsymbol{\eta}_a[k] - \hat{\boldsymbol{\eta}}[k]$ represents tracking errors for code, phase and frequency at epoch k. In this paper, the parameters $\boldsymbol{\eta}_a[k]$, $\Delta\boldsymbol{\eta}[k]$, and $\varepsilon_{\boldsymbol{\eta}}[k]$ are treated as deterministic. For clarity, the index k of $\varepsilon_{\boldsymbol{\eta}}[k]$ and $\Delta\boldsymbol{\eta}[k]$ is omitted in subsequent equations.

From Eqs. (5) and (4), the correlator output $\lambda[k]$ is a linear combination of the nominal ($\lambda_a[k]$), meaconing ($\lambda_s[k]$), and noise ($\lambda_n[k]$) correlations. In [11], a classification of the meaconer's impact on the correlator output is established based on the orthogonality properties of the PRN code as a function of the relative parameters $\Delta\boldsymbol{\eta}$: 1) jamming situation, where the nominal correlation is tracked and meaconing correlation is negligible ($\lambda^{(J)} = \lambda_a + \lambda_n$); 2) spoofing situation, where the meaconing correlation is tracked and nominal correlation is negligible ($\lambda^{(S)} = \lambda_s + \lambda_n$); and 3) multipath situation, where both the nominal and meaconing are considered in the correlator expression ($\lambda^{(M)} = \lambda_a + \lambda_s + \lambda_n$). The conditions on $\Delta\boldsymbol{\eta}$ to achieve each situation are detailed in [11]. Additionally, the nominal situation (without RFI) is considered.

3. REAL C/N_0

3.1. Instantaneous real C/N_0

The real C/N_0 is the C/N_0 faced by the receiver. It can be expressed from the instantaneous Signal-to-Noise Ratio (SNR), denoted $\rho[k]$ defined as the ratio between the useful signal power $P_d[k]$ and the noise power $P_n[k]$ at epoch k as

$$\rho[k] \triangleq \frac{P_d[k]}{P_n[k]} = \frac{\mathbb{E}\left[|\lambda_d[k]|^2\right]}{\mathbb{E}\left[|\lambda_n[k]|^2\right]}. \quad (6)$$

The useful signal $\lambda_d[k]$ is defined as the signal carrying the navigation message $d(t)$. Therefore $\lambda_d^{(J)} = \lambda_a$ in nominal and jamming situations, $\lambda_d^{(S)} = \lambda_s$ in spoofing situation and $\lambda_d^{(M)} = \lambda_a + \lambda_s$ in multipath situation.

Nominal:

In nominal conditions, $P_d^{(N)}[k] = \zeta(\varepsilon_{\boldsymbol{\eta}})^2 C_a$, and $P_n^{(N)} = N_0 \zeta_\tau(0)/T_i$, where $\zeta(\varepsilon_{\boldsymbol{\eta}}) = \zeta_\tau(\varepsilon_\tau)\zeta_f(\varepsilon_f)$ depicts the total synchronization mismatch losses, with ζ_τ and ζ_f the code

and frequency synchronization mismatch losses, defined as

$$\zeta_\tau(\varepsilon_\tau) \triangleq \int_{-B/2}^{B/2} G_c(f)e^{j2\pi f\varepsilon_\tau}df, \;\; \zeta_f(\varepsilon_f) \triangleq \text{sinc}\,(\pi\varepsilon_f T_i) \quad (7)$$

where $G_c(f)$ is the PRN signal PSD and B is the RFFE double-sided bandwidth. Considering synchronization mismatch ζ and RFFE degradation $\zeta_\tau(0)$, the C/N_0 can be expressed as $C/N_0 = \rho/T_i$ [12], therefore

$$\left(\frac{C}{N_0}\right)^{(N)} = \frac{\zeta(\varepsilon_{\boldsymbol{\eta}})^2}{\zeta_\tau(0)}\frac{C_a}{N_0}. \quad (8)$$

Jamming:

In the jamming situation, $P_d^{(J)}[k] = \zeta(\varepsilon_{\boldsymbol{\eta}})^2 C_a$, and $P_n = N_0(1 + \Delta N)\zeta_\tau(0)/T_i$, then

$$\left(\frac{C}{N_0}\right)^{(J)} = \frac{\zeta(\varepsilon_{\boldsymbol{\eta}})^2}{\zeta_\tau(0)}\frac{1}{1 + \Delta N}\frac{C_a}{N_0}. \quad (9)$$

Spoofing:

In the spoofing situation, $P_d^{(S)}[k] = \Delta g\,\zeta(\varepsilon_{\boldsymbol{\eta}} + \Delta\boldsymbol{\eta})^2 C_a$, and $P_n = N_0(1 + \Delta N)\zeta_\tau(0)/T_i$, then

$$\left(\frac{C}{N_0}\right)^{(S)} = \frac{\zeta(\varepsilon_{\boldsymbol{\eta}} + \Delta\boldsymbol{\eta})^2}{\zeta_\tau(0)}\frac{\Delta g}{1 + \Delta N}\frac{C_a}{N_0}. \quad (10)$$

Multipath:

In the multipath situation, $P_n = N_0(1 + \Delta N)\zeta_\tau(0)/T_i$ and $P_d^{(M)}[k] = |\zeta(\varepsilon_{\boldsymbol{\eta}}) + \sqrt{\Delta g}\,e^{j\Delta\theta}\zeta(\varepsilon_{\boldsymbol{\eta}} + \Delta\boldsymbol{\eta})|^2 C_a$, then

$$\left(\frac{C}{N_0}\right)^{(M)} = \frac{\left|\zeta(\varepsilon_{\boldsymbol{\eta}}) + \sqrt{\Delta g}\,e^{j\Delta\theta}\zeta(\varepsilon_{\boldsymbol{\eta}} + \Delta\boldsymbol{\eta})\right|^2}{\zeta_\tau(0)\,(1 + \Delta N)}\frac{C_a}{N_0}. \quad (11)$$

3.2. Average real C/N_0

The average real C/N_0 is defined as the mean value of real C/N_0 observed during an observation interval $T_0 = MT_i$. The average SNR during this observation period can be defined as

$$\overline{\rho} \triangleq \frac{\overline{P_d}}{\overline{P_n}} = \frac{\langle\mathbb{E}[\,|\lambda_d[k]|^2\,]\rangle}{\langle\mathbb{E}[\,|\lambda_n[k]|^2\,]\rangle}. \quad (12)$$

with $\langle\,\eta\,\rangle$, the time average of $\eta[k]$ over M epochs as

$$\langle\,\eta\,\rangle \triangleq \frac{1}{M}\sum_{k=0}^{M-1} \eta[k]. \quad (13)$$

In this work, the parameters $\Delta\boldsymbol{\eta}$ and $\varepsilon_{\boldsymbol{\eta}}$ are assumed to be constant within the observation period, except for the relative phase, which is considered to evolve linearly: $\Delta\theta[k] = \Delta\theta_0 + \pi\Delta f\,T_i(2k + 1)$, where $\Delta\theta_0$ defines the relative phase at the onset of the observation period. The noise component

$\lambda_n[k]$ is assumed to be Gaussian. Given the assumptions on the variation of $\Delta\boldsymbol{\eta}$ and $\varepsilon_{\boldsymbol{\eta}}$, the noise power remains constant over the observation period, as does the signal power, except in multipath situations. Therefore, the average power is equal to the instantaneous one, presented in Sec. 3.1. In the multipath situation, the instantaneous power $P_d^{(\mathrm{M})}[k]$ can be divided into a constant term $\mu_d = \zeta(\varepsilon_{\boldsymbol{\eta}})^2 + \Delta g\,\zeta(\varepsilon_{\boldsymbol{\eta}} + \Delta\boldsymbol{\eta})^2$ and an oscillation term defined by its time average ω_d and time variance $\sigma_d^2 = \Omega_d - \omega_d^2$, with

$$\omega_d = 2\sqrt{\Delta g}\,\zeta(\varepsilon_{\boldsymbol{\eta}})\zeta(\varepsilon_{\boldsymbol{\eta}} + \Delta\boldsymbol{\eta})\,\mathrm{sinc}_M(\Delta f T_{\mathrm{i}})\cos\left(\overline{\Delta\theta}\right)$$

and

$$\begin{aligned}\Omega_d = \;&2\,\Delta g\,\zeta(\varepsilon_{\boldsymbol{\eta}})^2\zeta(\varepsilon_{\boldsymbol{\eta}} + \Delta\boldsymbol{\eta})^2 \\ &\times\left(1 + \mathrm{sinc}_M(2\Delta f T_{\mathrm{i}})\cos\left(2\overline{\Delta\theta}\right)\right).\end{aligned} \quad (14)$$

with $\mathrm{sinc}_M(\Delta f\,T_{\mathrm{i}}) = \sin(\pi M \Delta f\,T_{\mathrm{i}})/(M\sin(\pi\Delta f\,T_{\mathrm{i}}))$ and $\overline{\Delta\theta} = \Delta\theta_0 + \pi M \Delta f\,T_{\mathrm{i}}$. The average power in multipath situation is expressed as $\overline{P_d}^{(\mathrm{M})} = (\mu_d + \omega_d)\,C_{\mathrm{a}}$.

4. C/N_0 ESTIMATORS DISTORTION

The estimate C/N_0 is obtained by the receiver from the correlation outputs exploitation. This section explores the influence of a meaconer on the MM and NWPR estimators. Each estimator is briefly described, and their theoretical behavior is derived. In this work, it is assumed that the estimation period (MT_{i}) is sufficiently long and the C/N_0 is sufficiently high ($C/N_0 > 30$ dB.Hz) to consider the receiver to be within its operational range, where both estimators are unbiased in nominal situations [3, 13].

4.1. Moment Method (MM)

The MM measures the second- and fourth-order moments, defined as $M_2 \triangleq \mathbb{E}[|\lambda|^2]$ and $M_4 \triangleq \mathbb{E}[|\lambda|^4]$, in order to estimate the signal power $\overline{P_d}$ and noise power $\overline{P_n}$. The receiver estimates the statistical moments with the time average over M integration times, resulting in $\hat{M}_2 = \langle\,|\lambda|^2\,\rangle$ and $\hat{M}_4 = \langle\,|\lambda|^4\,\rangle$. The C/N_0 can then be expressed as [3]

$$\widehat{\frac{C}{N_0}}_{\mathrm{MM}} = \frac{1}{T_{\mathrm{i}}}\frac{\sqrt{2\hat{M}_2^2 - \hat{M}_4}}{\hat{M}_2 - \sqrt{2\hat{M}_2^2 - \hat{M}_4}}. \quad (15)$$

The theoretical behaviour of the MM estimator can be approximated as [12]

$$\mathbb{E}\left[\widehat{\frac{C}{N_0}}\right]_{\mathrm{MM}} \approx \frac{1}{T_{\mathrm{i}}}\frac{\sqrt{2\,\mathbb{E}[\hat{M}_2]^2 - \mathbb{E}[\hat{M}_4]}}{\mathbb{E}[\hat{M}_2] - \sqrt{2\,\mathbb{E}[\hat{M}_2]^2 - \mathbb{E}[\hat{M}_4]}}. \quad (16)$$

The expectation of the second- and fourth-order moments can be calculated for all situations. In jamming and spoofing situations, where power remains constant, the calculations yield

$\mathbb{E}[\hat{M}_2] = P_n + P_d$ and $\mathbb{E}[\hat{M}_4] = 2P_n^2 + 4P_nP_d + P_d^2$. By inserting these values into (16), the resulting estimator behaviour aligns with the theoretical model equations (9) and (10). As a result, the meaconer does not induce additional bias in jamming, and spoofing situations. In the multipath situation, the expected values of the moments can be computed as $\mathbb{E}[\hat{M}_2] = P_n + \overline{P_d}^{(\mathrm{M})}$ and $\mathbb{E}[\hat{M}_4] = 2P_n^2 + 4P_n\overline{P_d}^{(\mathrm{M})} + (\overline{P_d}^{(\mathrm{M})})^2 + C_{\mathrm{a}}^2\sigma_d^2$. Therefore, inserting these values into (16), the estimator behaviour is

$$\mathbb{E}\left[\widehat{\frac{C}{N_0}}\right]_{\mathrm{MM}}^{(\mathrm{M})} \approx \frac{1}{T_{\mathrm{i}}}\frac{\sqrt{(\overline{P_d}^{(\mathrm{M})})^2 - C_{\mathrm{a}}^2\sigma_d^2}}{P_n + \overline{P_d}^{(\mathrm{M})} - \sqrt{(\overline{P_d}^{(\mathrm{M})})^2 - C_{\mathrm{a}}^2\sigma_d^2}}. \quad (17)$$

4.2. Narrowband-Wideband Power Ratio (NWPR)

The NWPR method estimates the C/N_0 by comparing the signal-plus-noise power in two distinct bandwidths. This involves the measurement of power in $1/T_c$ (wide-band power) and $1/NT_c$ (narrow-band power) noise bandwidths, which can be expressed as [10, p. 391]

$$\mathrm{WBP}_k \triangleq \sum_{i=0}^{N-1}|\lambda[i]|^2, \quad \mathrm{NBP}_k \triangleq \left|\sum_{i=0}^{N-1}\lambda[i]\right|^2 \quad (18)$$

with $N = T_{\mathrm{i}}/T_c$. The normalized power is then defined as $\mathrm{NP}_k = \mathrm{NBP}_k/\mathrm{WBP}_k$. The expectation of the normalized power is defined as $\mu_{\mathrm{NP}} = \mathbb{E}[\mathrm{NP}_k]$. The receiver estimates μ_{NP} by its time time average over MT_{i} as $\hat{\mu}_{\mathrm{NP}} = \langle\,\mathrm{NP}_k\,\rangle$ resulting in

$$\widehat{\frac{C}{N_0}}_{\mathrm{NWPR}} = \frac{1}{T_c}\frac{\hat{\mu}_{\mathrm{NP}} - 1}{N - \hat{\mu}_{\mathrm{NP}}}. \quad (19)$$

Within its operational range, the NWPR estimator behaviour can be approximated as [12]

$$\mathbb{E}\left[\widehat{\frac{C}{N_0}}\right]_{\mathrm{NWPR}} \approx \frac{1}{T_c}\frac{\mathbb{E}[\hat{\mu}_{\mathrm{NP}}] - 1}{N - \mathbb{E}[\hat{\mu}_{\mathrm{NP}}]} \quad (20)$$

with

$$\mathbb{E}[\hat{\mu}_{\mathrm{NP}}] \approx \frac{1}{M}\sum_{k=0}^{M-1}\frac{\mathbb{E}[\mathrm{NBP}_k]}{\mathbb{E}[\mathrm{WBP}_k]}. \quad (21)$$

In jamming and spoofing situations, where signal and noise power are constant, $\mathbb{E}[\mathrm{NBP}_k] = NP_n + N^2P_d$ and $\mathbb{E}[\mathrm{WBP}_k] = NP_n + NP_d$. Inserting these into (21) and (20) the estimator behaviour aligns with the theoretical real C/N_0 Eqs. (8), (9), and (10). Consequently, the meaconer does not induce additional bias in these situations. In multipath situation, $\mathbb{E}[\mathrm{NBP}_k] \approx NP_n + N^2P_d^{(\mathrm{M})}[k]$ and $\mathbb{E}[\mathrm{WBP}_k] = NP_n + NP_d^{(\mathrm{M})}[k]$. The time average in Eq. (21) can be developed through its second-order Taylor expansion, as outlined in [10, p. 391]. Subsequently, inserting this into (20), the theoretical estimator behaviour can be expressed as

$$\mathbb{E}\left[\widehat{\frac{C}{N_0}}\right]_{\mathrm{NWPR}}^{(\mathrm{M})} \approx \frac{1}{T_c}\frac{\overline{P_d}^{(\mathrm{M})} - P_n\sigma_d^2}{P_n\left(1 + \sigma_d^2\right)}. \quad (22)$$

5. SIMULATIONS

A simulated reception chain is implemented to compare the theoretical and simulated real C/N_0 (presented in Sec. 3.2), theoretical and simulated estimated C/N_0 (Sec. 4), as well as to compare real and estimated C/N_0 values. The simulation is conducted though three distinct scenarios: jamming, spoofing, and multipath. The simulated reception chain includes correlators, code and phase tracking loops, and C/N_0 estimation algorithms. The simulation parameters are $T_i = 20$ ms, $M = 50$, $T_c = 1$ ms and $N = 20$. The incoming signal is simulated from signal model Eq. (4). The nominal parameters $\boldsymbol{\eta}_a$ are generated to emulate a realistic dynamic geometry. The nominal C_a/N_0 is set to 45 dB.Hz. The tracking errors $\varepsilon_{\boldsymbol{\eta}}$ in the synchronization mismatch losses in Eq. (7) are generated based on the outcomes of the simulated tracking loops.

Fig. 1 presents results for the three scenarios. Theoretical and simulated real C/N_0 are shown in black. The simulated real C/N_0 is obtained from simulated correlator outputs by measuring separately noise and signal powers. The Moment (blue) and NWPR (purple) estimates are plotted. The relative parameters (red) differ for each simulated scenario and are generated from scenario-specific conditions detailed in [11]. In jamming and spoofing, a quadratic relative phase $\Delta\theta$ and code $\Delta\tau$ are chosen with a rate of $\dot{\Delta f} = 0.2$ Hz.s^{-1}, and Δg follows the curve in Fig. 1.a-b. In the multipath scenario, $\Delta g = 0.64$, and $\Delta\theta$ and $\Delta\tau$ are tailored to yield to Δf (in red in Fig. 1.c). Finally, in all scenarios, $\Delta N = \Delta g$.

Simulated jamming scenario:

In the jamming scenario (Fig. 1.a), the six curves for theoretical and simulated real and estimated C/N_0 values match perfectly, verifying the models and the unbiased behaviour of the estimators in this situation. Additionally, this scenario highlights the jamming effects of the meaconer, acting as a jammer, inducing a decrease in C/N_0 as predicted by Eq. (9).

Simulated spoofing scenario:

Similar to the jamming scenario, the six curves in the spoofing scenario (Fig. 1.b) align perfectly, confirming the accuracy of the models and the unbiased behaviour of the estimators. The receiver's tracking of the meaconing correlation is clear through the C/N_0 behaviour, aligning with Eq. (10). Specifically, for $\Delta g \ll 1$, $C/N_0 \approx \Delta g\, C_a/N_0$, and for $\Delta g \gg 1$, $C/N_0 \approx \frac{\Delta g}{\Delta N} C_a/N_0 = C_a/N_0$.

Simulated multipath scenario:

In the multipath scenario (Fig. 1.c), the theoretical and simulated C/N_0 match for both real and estimated values, confirming the validity of the theoretical models (Eqs. (11), (17), and (22)) and the assumptions made regarding $\Delta\boldsymbol{\eta}$ and $\varepsilon_{\boldsymbol{\eta}}$ in
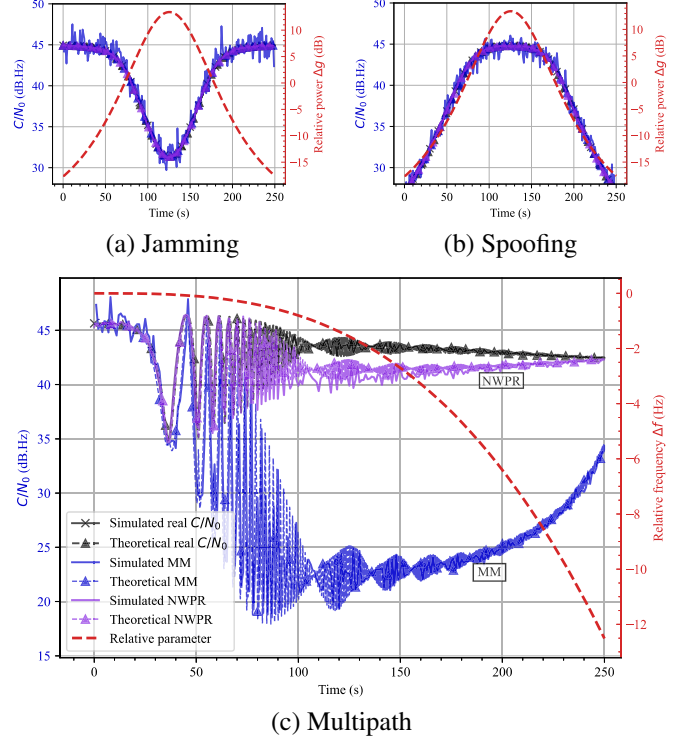

(a) Jamming   (b) Spoofing

(c) Multipath

Fig. 1. Comparison between simulated C/N_0 results and presented models (legend shared between subFigs.)

Sec. 4. However, this scenario also highlights a deviation between the real C/N_0 and estimated C/N_0. While the NWPR, measured from power measurements, experiences a decline of 3 dB ($\Delta f \approx 2$ Hz), MM, relying on overall signal variation, registers a reduction of over 21 dB.

6. CONCLUSION

This paper presents a characterization of the C/N_0 in the presence of a meaconer, considering a four-situation classification: nominal, jamming, spoofing, and multipath. A theoretical model of the real C/N_0 as well as the estimated C/N_0 by MM and NWPR algorithms has been developed. While the jamming and spoofing situations show no bias, the multipath situation shows a significant deviation between real and estimated C/N_0. The results presented in the context of meaconer situations are applicable to the corresponding types of interference, which include jamming, spoofing, and multipath. In summary, this paper deepens the comprehension of meaconer distortion on C/N_0 estimation. Future work with real meaconer signals could validate the models, and a deeper exploration of meaconer impact on other reception blocks could improve comprehension for future detection/mitigation techniques. In addition, the study of estimator variances in comparison to optimal bounds such as the Cramer-Rao Bound (CRB) or misspecified CRB [14] will be further investigated.

7. REFERENCES

[1] Michael S. Braasch and A.J. van Dierendonck, "GPS Receiver Architectures and Measurements," *Proc. of the IEEE*, vol. 87, no. 1, pp. 48–64, Jan 1999.

[2] Gustavo Lopez-Risueno and Gonzalo Seco-Granados, "C/N_0 Estimation and Near-Far Mitigation for GNSS Indoor Receivers," in *Proc. 2005 IEEE 61st Veh. Technol. Conf.*, May 2005, vol. 4, pp. 2624–2628.

[3] David R. Pauluzzi and Norman C. Beaulieu, "A Comparison of SNR Estimation Techniques for the AWGN Channel," *IEEE Trans. Commun.*, vol. 48, no. 10, pp. 1681–1691, Oct. 2000.

[4] Mark L. Psiaki and Todd E. Humphreys, "GNSS Spoofing and Detection," *Proc. of the IEEE*, vol. 104, no. 6, pp. 1258–1270, Apr. 2016.

[5] Todd E. Humphreys, Jahshan A. Bhatti, Daniel Shepard, and Kyle Wesson, "The Texas Spoofing Test Battery: Toward a Standard for Evaluating GPS Signal Authentication Techniques," in *Proc. 25th Int. Tech. Meeting Satell. Division of the Inst. of Navigation (ION GNSS)*, Nashville, TN, USA, Sep. 2012, p. 3569–3583.

[6] Kyle Wesson, Mark P. Rothlisberger, and Todd E. Humphreys, "Practical Cryptographic Civil GPS Signal Authentication," *Navigation*, vol. 59, no. 3, pp. 177–193, 2012.

[7] Damian Miralles, Aurelie Bornot, Paul Rouquette, Nathan Levigne, Dennis M. Akos, Yu-Hsuan Chen, Sherman Lo, and Todd Walter, "An Assessment of GPS Spoofing Detection Via Radio Power and Signal Quality Monitoring for Aviation Safety Operations," *IEEE Intell. Transp. Syst. Mag.*, vol. 12, no. 3, pp. 136–146, Jun. 2020.

[8] Ali Jafarnia Jahromi, Ali Broumandan, John Nielsen, and Gérard Lachapelle, "GPS Spoofer Countermeasure Effectiveness Based on Signal Strength, Noise Power, and C/N_0 Measurements," *Int. J. of Satell. Commun. and Netw.*, vol. 30, no. 4, pp. 181–191, 2012.

[9] Damian Miralles, Nathan Levigne, Dennis M Akos, Juan Blanch, and Sherman Lo, "Android Raw GNSS Measurements as the New Anti-Spoofing and Anti-Jamming Solution," in *Proc. of the 31st Int. Tech. Meeting of the Satell. Division of The Inst. of Navigation (ION GNSS+ 2018)*, Miami, Florida, USA, Sep. 2018, pp. 334–344.

[10] James J. Spilker Jr., Penina Axelrad, Bradford W. Parkinson, and Per Enge, *Global Positioning System: Theory and Applications, Volume I*, vol. 164, AIAA, 1996.

[11] Mathieu Hussong, Emile Ghizzo, Carl Milner, Axel Garcia-Pena, Julien Lesouple, and Christophe Macabiau, "Impact of Meaconers on Aircraft GNSS Receivers During Approaches," in *Proc. of the 36th Int. Tech. Meeting of the Satell. Division of The Inst. of Navigation (ION GNSS+ 2023)*, Sep. 2023.

[12] Emanuela Falletti, Marco Pini, and Letizia Lo Presti, "Low Complexity Carrier-to-Noise Ratio Estimators for GNSS Digital Receivers," *IEEE Trans. Aerosp. Electron. Syst.*, vol. 47, no. 1, pp. 420–437, Jan. 2011.

[13] Paul D. Groves, "GPS Signal-to-Noise Measurement in Weak Signal and High-Interference Environments," *Navigation*, vol. 52, no. 2, pp. 83–94, Feb. 2005.

[14] Lorenzo Ortega, Corentin Lubeigt, Jordi Vilà-Valls, and Eric Chaumette, "On GNSS Synchronization Performance Degradation under Interference Scenarios: Bias and Misspecified Cramér-Rao Bounds," *Navigation*, vol. 70, no. 4, 2023.